European Physical Journal E 20, 257 (2006) DOI: 10.1140/epje/i2005-10129-0

# Splay-bend textures involving tetrahedratic order

Harald Pleiner[1] [a], P.E. Cladis[2] and Helmut R. Brand[1,2,3]

[1] Max-Planck-Institute for Polymer Research, POBox 3148, 55021 Mainz, Germany;
[2] Advanced Liquid Crystal Technologies, POB 1314, Summit, NJ 07902, U.S.A.;
[3] Theoretische Physik III, Universität Bayreuth, 95440 Bayreuth, Germany.

Received: March 20, 2006

**Abstract.** We show that defect-free splay bend textures are less energetic compared to uniform states in liquid crystalline phases that possess both quadrupolar (nematic) and octupolar (tetrahedratic) order. This is because, in such systems, there is a symmetry allowed linear gradient term in the energy. Another unusual feature of these splay bend textures is the fact that they have a non homogeneous, space dependent free energy density. These results may help clarify some mysterious features noted for the B7 liquid crystal phase formed by achiral banana-shaped molecules.

**PACS.** 61.30.Gd Orientational order of liquid crystals; electric and magnetic field effects on order – 61.30.Dk Continuum models and theories of liquid crystal structure – 05.70.Ln Nonequilibrium irreversible thermodynamics

## 1 Introduction

Recently, tetrahedratic (octupolar) orientational order [1–3] has become an exciting topic for its potential relevance to liquid crystal phases formed by achiral banana shaped molecules [4–16]. Banana LC phases exhibit many peculiar properties and textures that elude understanding on the basis of only the usual liquid crystalline quadrupolar order. Figure 1 is an example of a myelin texture shown by the B7 phase of banana liquid crystals discovered by the Halle group [17]. We do not know the ground state of Weissflog's B7. Its x-ray diffraction is complex and does not reveal a simple structure, or indeed, any structure known up to now in quadrupolar liquid crystals. Here we give arguments for how the couplings between tetrahedratic and quadrupolar order could lead to an understanding of pictures, such as shown in Figure refmyelin, in terms of a biaxial nematic with an average length scale.

Radzihovsky and Lubensky [2] pointed out that a complete description of the symmetry of banana liquid crystals required, in addition to nematic order, ($Q_{ij}$, the quadrupolar mass density moment [18]), a third rank symmetric tensor order parameter, $T_{ijk}$ (derived from the octupolar mass density moment), as well as a vector order parameter, giving rise to a large number of new phases ranging from the well-known (pure) nematic liquid and the (pure) tetrahedratic liquid to novel biaxial, polar, and chiral phases [19].

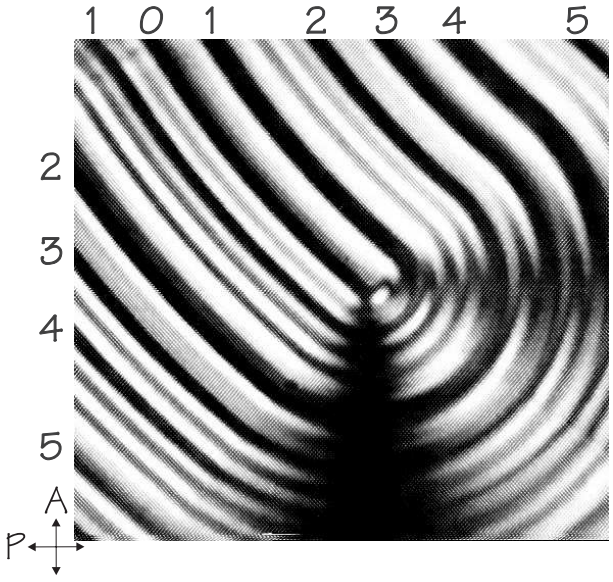


**Fig. 1.** Snapshot of a moving giant myelin, observed between crossed polarizers, in a free drop of B7 about $7K$ below the isotropic-B7 transition temperature [20]. The pattern is interpreted as splay-bend regions viewed perpendicular to the splay-bend plane. Remarkable features are thick continuous black lines, marked $1, 2, 3, ..$, and the weakly biaxial nature of the material as evidenced by the extinction asymmetry when one of the optic axes is perpendicular to the polarizer compared to when it is parallel to the polarizer. Average distance between black lines is $16.3 \pm 1.8 \mu m$. The field of view is $115 \times 123 \mu m^2$.

[a] e-mail: pleiner@mpip-mainz.mpg.de

Here, we disregard the vector order parameter and discuss specific effects when nematic and tetrahedratic order coexist. Such a coexistence is possible because, in general, the different moments of the mass distribution (the second moment for nematic, the third one for tetrahedratic order) are independent of each other. However, their gradient terms can couple at lower order [21] than the spatially homogenous terms [2]. As a result, visualization of the textures means depicting the spatially varying orientations of two independent order parameters. At this time, the molecular decoration of these structures is not known - even for the homogeneous state with all order parameters constant.

To explain some of the special effects exhibited by banana liquid crystals in general, Brand et al. discussed symmetry allowed cross-coupling terms between the various order parameters [21] as well as their coupling to external fields [22]. First they argued [22] that a coupling between the tetrahedral order parameter ($T_{ijk}$) and an electric field ($E_i$), could explain the observation of electric field induced flow ($\sigma_{jk} \sim T_{ijk}E_i$) in the optically isotropic phase [23,24] above the B7 - isotropic phase transition [17]. Indeed, by coupling to electric fields (but not magnetic fields), a tetrahedratic liquid can develop quadrupolar order ($Q_{jk} \sim T_{ijk}E_i$) [25].

Weissflog et al. found [26] that, with the application of an electric field, a liquid crystalline phase ($B2$ phase) could be induced in the optically isotropic phase up to about ten degrees above the thermodynamic phase transition temperature with the temperature shift being linear in the field strength. Assuming the optically isotropic phase to be the tetrahedratic one, this shift can be explained by bilinear energetic cross couplings between quadrupolar and octupolar order allowed in an external electric field ($\Delta f_t \sim T_{ijk}E_kQ_{jk}$) [21].

To account for ambidextrous chirality, the spontaneous formation of left- and right-handed twisted domains (ambidextrous chirality) in nematic [27–29] and smectic $C$-type [29] liquid crystal phases composed of achiral banana molecules, a symmetry allowed gradient term is needed [21].

The argument is the following. It is known that in a pure (achiral) nematic phase twist costs energy and the same is true for a pure (achiral) tetrahedratic phase. However, if both types of order are present, a bilinear energetic coupling term between quadrupolar and octupolar order involving a gradient (linear gradient term) allows for an energy reduction (compared to the homogeneous state) for a spontaneous counter-rotating twist structure of nematic and tetrahedratic order ($\Delta f_{grad} \sim T_{ijk}\nabla_k Q_{ij}$) [21].

Additional cross coupling and gradient terms in the reversible and dissipative dynamics have also been explored [30]. We find, for example, that crossed electric and temperature gradient fields lead in a tetrahedratic phase to an electric current perpendicular to both external forces, and spatial variations of the tetrahedratic order, as can arise near phase transitions, generate reversible stresses and can induce flow.

In this paper, we show that the linear gradient term present in any phase with both nematic and tetrahedratic order, not only allows spontaneous twist structures [21], but also splay-bend textures in both types of order. Such textures are local energy minima of a generalized energy. In addition, the splay-bend textures are biaxial whereas in the case of counter-rotating helices [21] the symmetry is uniaxial. We will argue that spontaneous splay-bend could give a minimal description to understand nearly all features shown in Figure 1 which is a signature of Weissflog's B7.

In systems with only nematic order, splay-bend textures always cost more energy than a uniform state. This is also qualitatively different from that encountered in a polar nematic with a (pure) splay phase [31] that necessarily involves defects. This result could also give some physical basis for the incredible variety of time dependent textures observed in achiral banana liquid crystals, for example, as have been described by Coleman et al. and which they attribute to an *ad hoc* splay of a 2-dimensional director field [32].

In Sec.2 and Appendix A we give the mathematical description of splay-bend textures. We investigate in detail two cases, first, rotations of the nematic director are confined to a plane (2D case, Sec.2.1), while in the second one, (3D case, Sec.2.2), it has an out-of-plane component. The rotations of the tetrahedratic orientations always form a 3D pattern. Depending on the actual values of some rotational elastic moduli, the 2D or the 3D structure has the lower energy. The structures minimizing the free energy show a spatially varying energy density.

The special case of a homogeneous energy density, presented in Appendix B, when the angle, $\phi$, between the splay-bend rotation axis of tetrahedral order and that of quadrupolar order is constrained to be such that $cos\phi = \pm 1/3$, turns out to be slightly more energetic than those with spatially varying energy densities. In contrast, spatially varying energy densities corresponding to a local minimum are characterized by a weak, spatially varying biaxiality.

In Sec.3.1 we visualize the bend-splay texture and discuss the possible relation of the spontaneous splay-bend texture to actual experimental findings on myelinic growth patterns. While spontaneous counter-rotating helices [21] of nematic-tetra order may account for the proliferation of uniaxial myelins in the mysterious B7 phase of banana liquid crystals, biaxial myelins (Figure 1) require spontaneous splay-bend to account for their optical biaxiality.

## 2 Splay-bend texture

In this section we show that, due to a linear gradient term [21] in the energy involving both nematic and tetrahedratic order, a splay-bend texture in the nematic director, $\mathbf{n}$, coupled to a similar texture in the tetrahedratic unit vectors $n_i^a$ (with $a = 1, 2, 3, 4$) has lower energy than a spatially homogeneous state.

We consider two nematic splay-bend configurations: a two-dimensional one

$$\mathbf{n} = (\cos qx, \sin qx, 0) \tag{1}$$

for the director in the (x,y)-plane, and a three-dimensional one

$$\mathbf{n} = (\beta \cos qx, \beta \sin qx, \alpha) \tag{2}$$

with $\alpha^2 + \beta^2 = 1$. Here the value of the wave vector, $q$, is a parameter to be evaluated later.

For the four unit vectors, $n_i^a$, characterizing tetrahedratic order we start with the configuration

$$\mathbf{n^1} = \frac{1}{\sqrt{3}}(1, -1, 1) \tag{3}$$

$$\mathbf{n^2} = \frac{1}{\sqrt{3}}(1, 1, -1) \tag{4}$$

$$\mathbf{n^3} = \frac{1}{\sqrt{3}}(-1, -1, -1) \tag{5}$$

$$\mathbf{n^4} = \frac{1}{\sqrt{3}}(-1, 1, 1) \tag{6}$$

which is very similar to the configuration used by Fel [1]. The $\mathbf{n}^a$ are at an angle $\psi$ with $\cos\psi = -1/3$ ($\psi = 109.47°$) to each other.

First we also assume a periodic structure of the $n_i^a$ rotating them by an angle $kx$ around the $z$ axis, where the wavelength $k$ will be determined later. In a final step we rotate this set of $n_i^a$ by a constant angle $\phi$ around the $y$ axis, where the angle $\phi$ is at this stage also a free parameter. Details of the rotations and explicit expressions for the rotated tetrahedral unit vectors are given in Appendix A. Visualization of the final structure is provided in Sec.3.1.

Thus, we have a total of four parameters characterizing the spatial variations of quadrupolar and tetrahedratic order: $q$ is associated with the characteristic wave vector for spatial variations of $\mathbf{n}$, $\beta = 1$ or $\neq 1$ governs the dimensionality of that structure, while $k$ and $\phi$ characterize the wave vector of the tetrahedral order, and its orientation relative to the quadrupolar order.

To check the energy change of the splay-bend texture relative to the homogeneous state, we analyze the energy up to quadratic order in the gradients:

$$F = F_0 + \int dV \left( \mathcal{D} T_{ijk} \nabla_k Q_{ij} + \gamma (\nabla_k Q_{ij})^2 + \delta (\nabla_k T_{ijl})^2 \right) \tag{7}$$

where $Q_{ij} = \frac{S}{2}(3 n_i n_j - \delta_{ij})$ is the orientational order parameter with $S$ its modulus and $T_{ijk} = \sum_{a=1}^{4} n_i^a n_j^a n_k^a$ (with $T_{ikk} = 0$) is the tetrahedratic order parameter, while $F_0$ contains the spatially homogeneous terms in $T_{ijk}$ and $Q_{ij}$. The modulus of the tetrahedratic order parameter has been set to 1 without loss of generality. We can keep the order parameter moduli $S$ and $T$ constant as we are not close to a phase transition and the structures considered are defect-free. One also note that an energy contribution $\sim Q_{ij} \nabla_k T_{ijk}$ differs only by a surface term from that taken into account in Eq.(7). The various components of $T_{ijk}$ and $Q_{ij}$ for the splay-bend texture are calculated in Appendix A.

For the nematic contribution to the gradient energy we obtain using Eqs.(A.20)-(A.25)

$$\gamma (\nabla_k Q_{ij})^2 = \frac{9}{2} \gamma \, S^2 q^2 \beta^2. \tag{8}$$

In the two-dimensional case, $\beta = 1$. Similarly, for the tetrahedratic contribution to the gradient energy, we obtain, using Eqs.(A.11)-(A.19),

$$\delta (\nabla_k T_{ijl})^2 = \frac{32}{9} \delta \, (2k)^2. \tag{9}$$

For the linear gradient term $\sim \mathcal{D}$, we have for the splay-bend texture:

$$\begin{aligned} \mathcal{D} T_{ijk} \nabla_k Q_{ij} = \frac{2}{\sqrt{3}} \mathcal{D} S q \Big( & \big[ 4 \cos\phi \cos(2kx) \cos(2qx) \\ & - (1 + 3\cos^2\phi) \sin(2kx) \sin(2qx) \big] \beta^2 \sin\phi \\ & - \big[ \cos\phi (-1 + 3 \sin^2\phi) \sin(2kx) \sin(qx) \\ & + \cos(2\phi) \cos(2kx) \cos(qx) \big] 2\alpha\beta \Big). \end{aligned} \tag{10}$$

Now we are ready to analyse the question to what extent the contribution of the linear gradient term given in Eq.(10) can lower the energy in the presence of a splay-bend distortion.

To do this we focus on the large aspect-ratio limit, meaning that we are looking at length scales, $L$, large compared to the wavelengths $2\pi/q$ and $2\pi/k$ associated with splay-bend distortions. Inspecting Eqs.(8) and (9), we see that both contributions are independent of space and are just multiplied by the system size ($L$) when calculating the total energy from the energy density. In addition, both contributions are also independent of the angle $\phi$.

In the following analysis, we therefore concentrate on the effects of the linear gradient contribution given in Eq.(10) and address the question to what extent this term can give rise to a lower energy when compared to a spatially homogeneous solution for $Q_{ij}$ and $T_{ijk}$.

### 2.1 Two-dimensional director structure

We first analyze the case of a two-dimensional director structure, i.e. $\beta = 1$, $\alpha = 0$ in Eq.(10). Integrating this energy density over $x$ (say from 0 to $L$) we get a contribution proportional to $L$ for $k = \pm q$, only

$$\begin{aligned} & \frac{1}{L} \int_0^L \mathcal{D} T_{ijk} \nabla_k Q_{ij} dx \\ & = -\frac{1}{\sqrt{3}} \mathcal{D} S q \sin\phi [(1 + 3\cos^2\phi) \mp 4 \cos\phi] \end{aligned} \tag{11}$$

while all contributions for $k \neq \pm q$ are $\sim O(1/L)$ and oscillatory in $L$ and vanish in the limit of large $L$. Minimizing

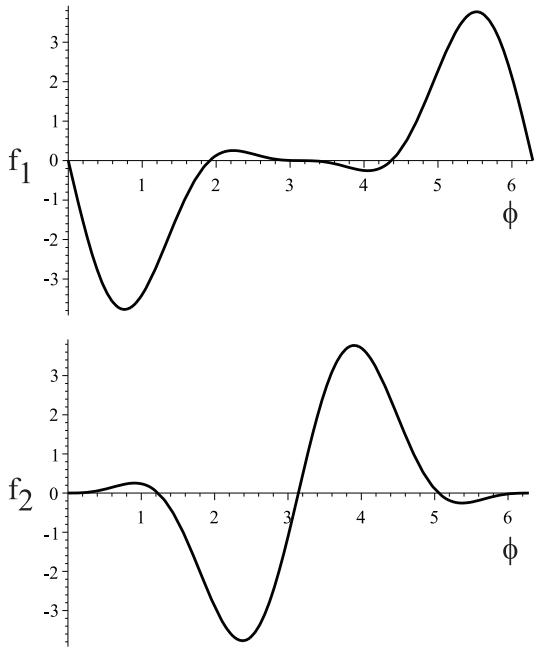


**Fig. 2.** This plot shows the energy due to the linear gradient term, Eq.(11), in units of $\mathcal{D}Sq/\sqrt{3}$ as a function of the angle $\phi$ in radians. On top the case $k = -q$ is plotted and at the bottom $k = q$. We note that the values at the extrema are equal in magnitude. See text for detailed positions of the extrema.

Eq.(11) (the other energy contributions do not depend on $\phi$) with respect to $\phi$ we obtain the condition

$$\pm 4 - 5\cos\phi \mp 8\cos^2\phi + 9\cos^3\phi = 0. \tag{12}$$

For $k = q$, Eq.(12) takes the form

$$4 - 5\cos\phi - 8\cos^2\phi + 9\cos^3\phi = 0 \tag{13}$$

which has three solutions

$$\begin{aligned} \cos\phi_1 &= 1 \\ \cos\phi_{2,3} &= \frac{1}{18}(-1 \pm \sqrt{145}) \end{aligned} \tag{14}$$

leading to $\cos\phi_2 \approx 0.613$ and $\cos\phi_3 \approx -0.725$. The corresponding values for the *sin* are $\pm\sin\phi_2 \approx 0.790$ and $\pm\sin\phi_3 \approx 0.689$, where the signs of the value for the *sin* have to be chosen such that the linear gradient term leads to an energy reduction.

For $\mathcal{D} > 0$ and $\phi_2$, we obtain for the energy reduction due to the linear gradient term

$$\begin{aligned} &\frac{1}{L}\int_0^L \mathcal{D}T_{ijk}\nabla_k Q_{ij}dx \\ &\approx -0.148\mathcal{D}Sq \end{aligned} \tag{15}$$

while for $\mathcal{D} > 0$ and $\phi_3$, we have

$$\begin{aligned} &\frac{1}{L}\int_0^L \mathcal{D}T_{ijk}\nabla_k Q_{ij}dx \\ &\approx -2.178\mathcal{D}Sq. \end{aligned} \tag{16}$$

The latter case, corresponding to the larger energy reduction, is associated with an angle $\phi_3 \approx 2.381$ or $\phi_3 \approx 136.4°$. This result for $\mathcal{D} > 0$ corresponds to the deep well in $f_2$ of Figure 2. For $\mathcal{D} < 0$, one must choose $\sin\phi_3 \approx -0.689$ to get the biggest energy reduction to obtain for the angle, $\phi_3$, $\phi_3 \approx 3.902$ or $\phi_3 \approx 223.6°$ corresponding to the large peak in $f_2$ of Figure 2.

In Eq.(12), the case $k = -q$ is mapped to $k = q$ by shifting $\phi \to \phi + \pi$ resulting in the two energy minima being at $\phi \approx 5.523$ or $\approx 316.4°$ (for $\mathcal{D} > 0$) and $\phi \approx 0.760$ or $\approx 43.6°$ (for $\mathcal{D} < 0$) corresponding to the two extrema in $f_1$ of Figure 2.

Thus we obtain in all four cases an energy reduction due to the linear gradient term by $\approx -2.178|\mathcal{D}|Sq$ indicating that these four cases are degenerate and physically completely equivalent.

Minimization of the total free energy Eq.(7) with respect to the wave vector, $q$, gives the result

$$q_c \approx 1.089\frac{|\mathcal{D}|S}{\frac{9}{2}\gamma S^2 + \frac{128}{9}\delta} \tag{17}$$

which is a wave vector directly proportional to $|\mathcal{D}|$, or, equivalently, a length scale that diverges for $\mathcal{D} \to 0$. Inserting the value for $q_c$ in Eq.(7) we find an energy reduction,

$$\Delta F \approx -1.186\frac{\mathcal{D}^2 S^2}{\frac{9}{2}\gamma S^2 + \frac{128}{9}\delta} \tag{18}$$

independent of the sign of $\mathcal{D}$.

The energy minimum found above corresponds to a structure, whose energy density is spatially inhomogeneous. It is noteworthy that there exists also a spatially varying splay-bend deformation, which leads to a spatially *constant* energy density. This structure is discussed in Appendix B. Although having a slightly higher total energy than the structure discussed above, it is special, because the rotation angle $\phi$ in that structure is precisely the tetrahedral or dihedral angle.

The case of splay-bend deformations is different from that of pure twist studied in ref. [21] as, in the twist case, the contribution to the energy density due to the linear gradient term is independent of spatial coordinates (an invariant) for a particular choice of the helical wave vectors which is also the energy minimum. In addition, the energy is not further decreased by additional rotations about axes other than the helix axis.

In the case of splay-bend deformations, when integrated over an interval $L$ there is a finite energy reduction due to the linear term in the gradient energy density, even larger than that associated with the special structure having a spatially homogeneous energy density. In addition, a further energy reduction can be obtained - under certain circumstances - if the director is rotated additionally out of the plane, as we will discuss now.

### 2.2 Three-dimensional director texture

The goal is again to find structures that lead to a negative energy contribution resulting from the coupling en-

ergy density Eq.(10), now for $\beta \neq 1$. It is straightforward to show, along the lines of the preceding subsection, that for $k = \pm q$ no further energy reduction is obtained compared to the two-dimensional case $\beta = 1$. However, it is possible in the three-dimensional case to get a negative energy contribution proportional to $L$ for $q = \pm 2k$: for every $\pi$-rotation of the tetrahedra, the director rotates by $2\pi$. For that case,

$$\frac{1}{L}\int_0^L \mathcal{D}T_{ijk}\nabla_k Q_{ij}dx = -\frac{2}{\sqrt{3}}\mathcal{D}Sq\alpha\beta \times\left(\pm\cos\phi[-1+3\sin^2\phi]+1-2\sin^2\phi\right). \quad (19)$$

Minimizing with respect to $\phi$ leads to six values for $\cos\phi$: $\cos\phi_{1,2} = \pm 1$ and $\cos\phi_{3,4,5,6} = \pm(2\pm\sqrt{22})/9$. This result gives rise to

$$\frac{1}{L}\int_0^L \mathcal{D}T_{ijk}\nabla_k Q_{ij}dx = -\frac{4}{\sqrt{3}}|\alpha\beta\mathcal{D}|Sq \quad (20)$$

for both $\cos\phi_1$ and $\cos\phi_2$, while the prefactors for the other four solutions are smaller thus giving rise to a smaller energy reduction. Therefore we focus from now on on the effects associated with $\phi_1 = 0$ and $\phi_2 = \pi$.

For the total gradient energy (7) we obtain in the present case

$$F = \frac{9}{2}\gamma S^2 q^2\beta^2 - |\alpha\beta\mathcal{D}|SqN_3 + \frac{32}{9}\delta q^2 \quad (21)$$

with $N_3 = 4/\sqrt{3} \approx 2.309$. Minimizing Eq.(21) with respect to $q$ we get

$$q_c = \frac{|\alpha\beta\mathcal{D}|N_3 S}{9\beta^2\gamma S^2 + \frac{64}{9}\delta} \quad (22)$$

and for the total energy

$$F = -\frac{1}{2}\frac{\alpha^2\beta^2\mathcal{D}^2 N_3^2 S^2}{9\beta^2\gamma S^2 + \frac{64}{9}\delta}. \quad (23)$$

Minimization of Eq.(23) with respect to $\beta^2$ taking into account $\alpha^2 = 1-\beta^2$ leads to $\beta_c^2 = (-B+\sqrt{B^2+BA})/A$ with $2A = 9\gamma S^2$ and $9B = 32\delta$. Inserting this result for $\beta_c^2$ into Eq.(23) we find for the total energy for the 3 D case

$$F = -\frac{1}{4}\mathcal{D}^2 N_3^2 S^2 \frac{2B+A-2\sqrt{B^2+BA}}{A^2} \quad (24)$$

giving the energy reduction compared to the homogeneous, texture-free state.

This expression has to be compared with Eq.(18) for the 2D case, which reads in the present notation

$$F = -\frac{1}{4}\mathcal{D}^2 N_2^2 S^2 \frac{1}{A+4B} \quad (25)$$

with $N_2 \approx 2.178$. Comparing the two energies given in Eqs.(24) and (25) for 3D and 2D, respectively, we find that for $\approx 0.003 < B/A <\approx 2.259$ the 'arceau-type' 2D structures for the nematic director (studied in section 2.1) lead to a larger energy reduction, while outside this interval the 3D structures studied here (where the director rotates $2\pi$ for every $\pi$ rotation of the tetrahedra), are energetically preferred.

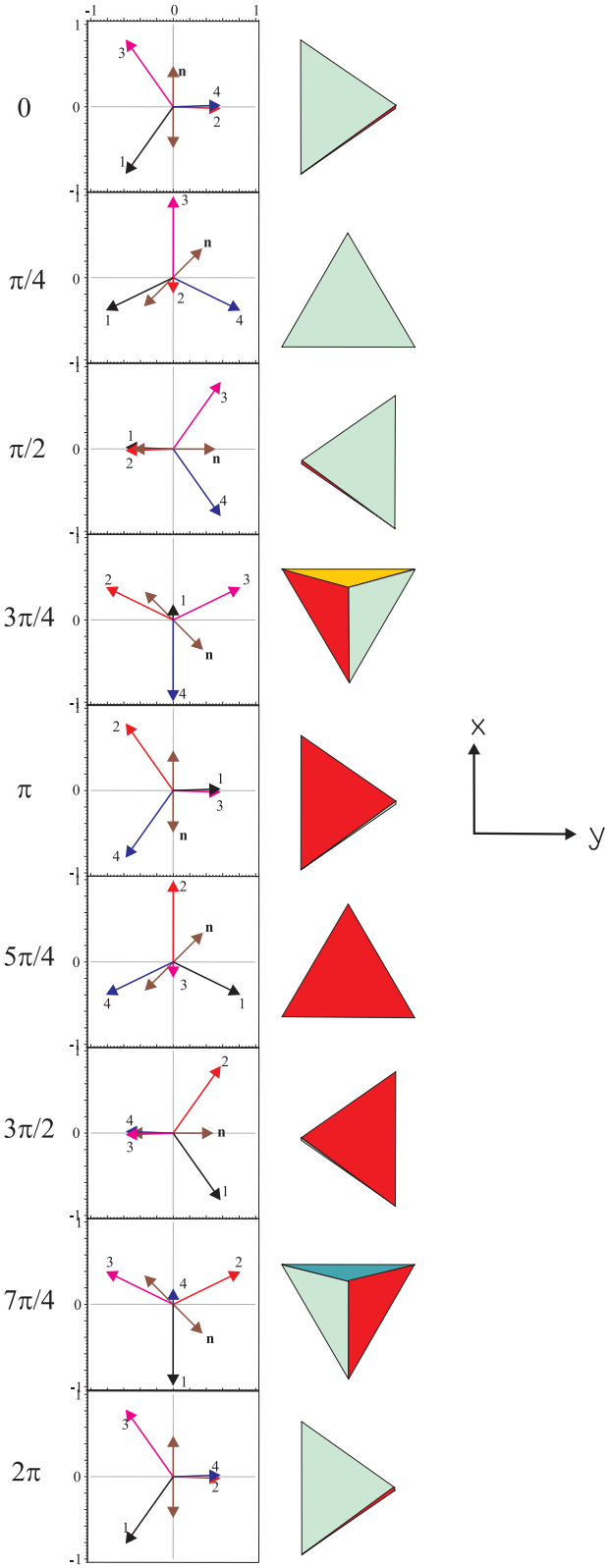


**Fig. 3.** The orientation of the tetrahedra in the splay-bend texture viewed along the z direction (right) and the projection of the tetrahedral unit vectors (labeled 1 to 4), and of the director **n**, in the (x,y)-plane (left) for different values of $kx$.

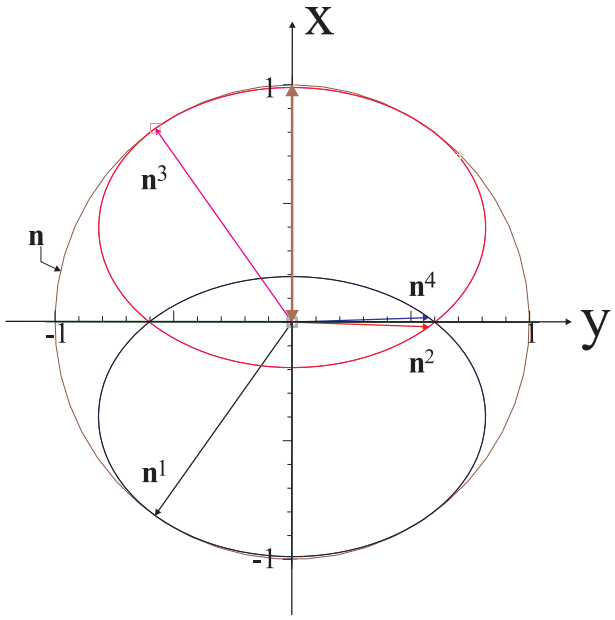


**Fig. 4.** Phase portrait ($0 \leq kx \leq 2\pi$) of the 2D director $\mathbf{n}$ and the tetrahedral unit vectors $\mathbf{n}^a$ of the splay-bend texture in the (x,y)-plane. The lines with arrows are for $kx = 0$, see text and Figure 3.

## 3 Visualization of the splay-bend texture

### 3.1 Visualisation: Geometric considerations

To build intuition, we now graphically analyze the results of the last section. The pattern is periodic in the $x$ direction and the orientations of the director and the tetrahedral unit vectors repeat after every $2\pi$ completion of the "phase" $kx$. In Figure 3 we show on the right the orientation of the tetrahedral unit vectors (the corners of the tetrahedra) looking along the $z$ axis for the phases $kx = m\pi/4$ ($m$ integer). On the left, the projection on the (x,y)-plane of these unit vectors is displayed. The vectors $\mathbf{n}^2$ and $\mathbf{n}^3$ always point into the plane, except for $kx = 5\pi/4$ and $kx = \pi/4$, respectively, while $\mathbf{n}^1$ and $\mathbf{n}^4$ always point out of the plane, except for $kx = 7\pi/4$ and $kx = 3\pi/4$, respectively. The actual drawing is done for the case of a 2D structure (the nematic director is in the (x,y)-plane) with $k = q$ and $\phi = 136.4°$. As it is clear from Figure 3, the tetrahedra break left - right symmetry in the planes perpendicular to $\hat{\mathbf{n}}$.

In the $xy$-projection, the tips of the unit vectors (and of the director) draw a closed path, when the phase $kx$ varies from 0 to $2\pi$. Such a phase portrait is shown in Figure 4. The director $\mathbf{n}$ performs a circle of radius $\beta$, while the tetrahedral unit vectors rotate on two identical ellipses with large and small axes of $(2/3)^{1/2}$ and $(2/3)^{1/2}|\cos\phi|$, respectively, and whose centers are shifted by $\pm(1/3)^{1/2}\sin\phi$ along the $x$-direction. Again, Figure 4 is done for $\phi = 136.4°$ and $\beta = 1$.

In Figure 5 we show a different perspective of the splay-bend texture, where it is rather simple. Instead of looking along the $z$- axis as in Figure 4, in Figure 5a, we look in the

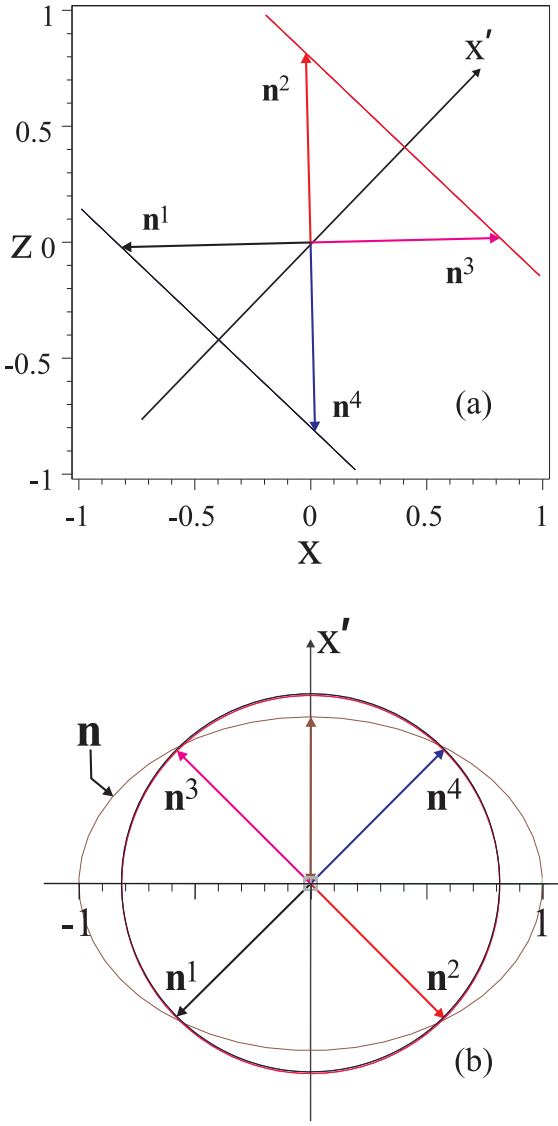


**Fig. 5.** Phase portrait of the tetrahedral unit vectors $\mathbf{n}^a$ of the splay-bend texture (a) viewed in the (x,z)-plane and (b) viewed in the (x',y)-plane which shows the uniform rotation of the $\mathbf{n}^1$-$\mathbf{n}^4$ 2-fold axis on one circle superimposed on that of $\mathbf{n}^2$-$\mathbf{n}^3$ 2-fold axis. The phase portrait of the 2D director, $\mathbf{n}$, is shown in (b) but not in (a). The $x'$-axis is a $\phi$-rotation of the $x$-axis. In this example, $\phi \sim -136°$. As in Figs. 3 and 4, the lines with arrows are for $kx = 0$.

(x'z)-plane, while in Figure 5b, the (x,y)-plane is rotated $-\phi$ around the $y$-axis to look along the pair of tetrahedral 2-fold axes. The phase portrait in this new (x',y)-plane consists of identical circles (of radius $(2/3)^{1/2}$) for the tetrahedral unit vectors and an ellipse for the director with long and short axis of $\beta$ and $\beta|\cos\phi|$, respectively, its center shifted by $\alpha\sin\phi$ along the $x'$ axis. Actually shown is the 2D case ($\alpha = 0$) for $\cos\phi = -0.725$. From this viewing angle, the phase portrait shows a uniform rotation of the tetrahedratic unit vectors.

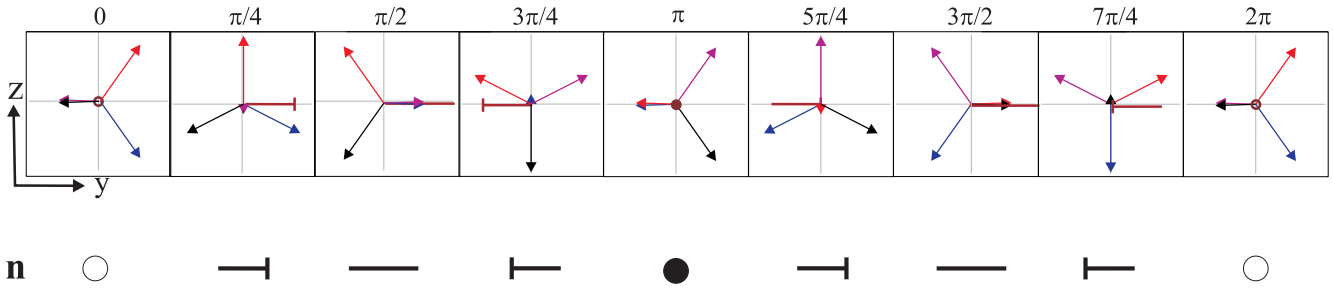


**Fig. 6.** One cycle of the biaxial splay-bend texture in $\pi/4$ intervals viewed looking into the $\hat{\mathbf{x}}$-axis. In the biaxial arceau, the tetrahedra break the left-right symmetry in the planes perpendicular to $\hat{\mathbf{n}}$. Below is the "nail" representation of a uniaxial splay bend texture viewed in the same direction.

### 3.2 Myelinic growth patterns observed in B7

The myelin texture has a "soft" length scale and can (and does) add or subtract non-integral multiples of wavelengths nearly continuously. This is in contrast to defect structures in systems with a "hard" length scale, e.g. dislocation lines in chiral systems, where the creation of additional lines can only be done in integral steps. Adding to the "softness" of this pattern and, in contrast to chiral systems, the splay-bend deformation calculated here has no preferred sense of rotation for splaying and bending. We now argue that the picture shown in Figure 1 can be interpreted as a spontaneous splay-bend texture with an average length scale.

Figure 6 shows the biaxial nature of the coupled tetrahedral and quadrupolar axes. The uniaxial director field is shown below using the convention that the end with the bar is in front of the plane. However, what is noticed is that the composite figure, uniaxial nail and isotropic tetrahedral vectors, is weakly biaxial. The coupling we have discussed is a new mechanism for creating biaxial objects: coupling a uniaxial field to a tetrahedral field at an angle that does not coincide with one of the tetrahedral principal axes makes the combined object biaxial.

Figure 1 shows a series of bright and dark lines. The very dark lines have numbers attached. The line "0" ends at a biaxial defect line perpendicular to the plane. The other marked lines can be followed around the defect line without interruption and splits into two dark lines along P in Figure 1. Dark lines all around the defect line means that an optic axis is also perpendicular to the plane - as in Figure 6 shown for 0, $\pi$ and $2\pi$.

The biaxial nature of this pattern is revealed by the different extinction brushes along the lines parallel and perpendicular to the polarizers set parallel and perpendicular to the edges of the picture. In a uniaxial system, these brushes are equally black. In Figure 1, one of the extinction brushes is zig-zaggy while the other is very dark. The very dark brush is associated with an optic axis that is close to being "ordinary" (weakly biaxial) so travels straight through the material unrefracted. The extraordinary ray refracts to minimize its trajectory along paths with spatially varying indices of refraction, and can even separate into two rays [33] as it does here when the splay-bend structure is illuminated with light polarized parallel to the polarizer (only one extraordinary ray). In such situations there is always some "focusing effect" that contributes to the intensity variation of "dark" lines around the defect and the bright white spot to the right of the intersection of line "0" and the nearly ordinary extinction brush.

Therefore we associate every dark line in Figure 1 with a director perpendicular to the plane. Between each of these dark lines, is a 0-$\pi$–splay-bend wall (also known as a *Bouligand arceau*). But this is a biaxial arceau.

As a result, Figure 1 may be the first observation of a biaxial nematic defect, predicted to come in three flavors [34]. Studies of the other allowed couplings discussed here may well lead to discoveries of the complete group of biaxial disclination patterns.

## 4 Conclusions and perspective

We have analyzed some of the consequences of the lowest order symmetry allowed coupling between spatial gradients in uniaxial quadrupolar and tetrahedral order and showed that it leads to several lower energy configurations compared to any uniform state. A prediction of this result is that when both quadrupolar and tetrahedral order are present, there can be no global uniform state. *A fortiori*, in the presence of tetrahedral and quadrupolar order, building blocks of the structure cannot reduce their energy by annealing or coalescing to form bigger objects. Out of equilibrium, they can grow or die but there will only be spatially varying building blocks filling up space because of the nature of these solutions (see, for example, the discussion in section 2.1).

Until the recent observations of biaxial nematic phases [35,36], nematic phases formed by banana-shaped molecules were found to be uniaxial [12,27]. However, nematic phases, regardless whether they are uniaxial or biaxial, have no macroscopic length scale. Here we have shown that coupling a direction to tetrahedral order can result in a biaxial nematic with an average length scale even without layering.

Our model provides a minimal physical picture for the myelinic growth patterns observed in Weissflog's B7 phase. It can be generalized to other liquid crystalline phases for which quadrupolar and tetrahedratic order coexist. Candidates include smectic phases formed by banana-shaped

achiral molecules and biologically relevant lipid-water lyotropic liquid crystals.

*Acknowledgments:* It is a pleasure for H.R.B. to thank the Deutsche Forschungsgemeinschaft for partial support of this work through Sonderforschungsbereich 481 'Polymere und Hybridmaterialien in inneren und äußeren Feldern'. We thank the Institute for Mathematics and its Applications (IMA), University of Minnesota, Minneapolis, USA, for their hospitality during part of this work. P.E.C. thanks the Alexander von Humboldt Foundation for the award of a Humboldt Research Prize, the University of Bayreuth and the Max-Planck-Institute for Polymer Research for support and hospitality during part of this work.

## Appendix A: Order Parameter tensors for the splay-bend texture

In this Appendix we calculate the components of the tetrahedratic and nematic order parameters for the splay-bend texture. First we rotate the $\mathbf{n}^a$, Eq.(3)-(6), by an angle $kx$ around the $z-$axis using the rotation matrix

$$\mathcal{R}_z = \begin{pmatrix} \cos kx & \sin kx & 0 \\ -\sin kx & \cos kx & 0 \\ 0 & 0 & 1 \end{pmatrix} \tag{A.1}$$

and obtain

$$\mathbf{n^1} = \frac{1}{\sqrt{3}}(\cos kx - \sin kx, -\sin kx - \cos kx, 1) \tag{A.2}$$

$$\mathbf{n^2} = \frac{1}{\sqrt{3}}(\cos kx + \sin kx, -\sin kx + \cos kx, -1) \tag{A.3}$$

$$\mathbf{n^3} = \frac{1}{\sqrt{3}}(-\cos kx - \sin kx, \sin kx - \cos kx, -1) \tag{A.4}$$

$$\mathbf{n^4} = \frac{1}{\sqrt{3}}(-\cos kx + \sin kx, \sin kx + \cos kx, 1). \tag{A.5}$$

Then we rotate this set of $\mathbf{n}^a$ by a fixed angle $\phi$ around the $y$ axis using the rotation matrix

$$\mathcal{R}_y = \begin{pmatrix} \cos\phi & 0 & -\sin\phi \\ 0 & 1 & 0 \\ \sin\phi & 0 & \cos\phi \end{pmatrix} \tag{A.6}$$

to get finally

$$\begin{aligned} \mathbf{n^1} = \frac{1}{\sqrt{3}} \; & (\cos\phi[\cos kx - \sin kx] - \sin\phi, \\ & -\sin kx - \cos kx, \\ & \sin\phi[\cos kx - \sin kx] + \cos\phi) \end{aligned} \tag{A.7}$$

$$\begin{aligned} \mathbf{n^2} = \frac{1}{\sqrt{3}} \; & (\cos\phi[\cos kx + \sin kx] + \sin\phi, \\ & -\sin kx + \cos kx, \\ & \sin\phi[\cos kx + \sin kx] - \cos\phi) \end{aligned} \tag{A.8}$$

$$\begin{aligned} \mathbf{n^3} = \frac{1}{\sqrt{3}} \; & (\cos\phi[-\cos kx - \sin kx] + \sin\phi, \\ & \sin kx - \cos kx, \\ & \sin\phi[-\cos kx - \sin kx] - \cos\phi) \end{aligned} \tag{A.9}$$

$$\begin{aligned} \mathbf{n^4} = \frac{1}{\sqrt{3}} \; & (\cos\phi[-\cos kx + \sin kx] - \sin\phi, \\ & \sin kx + \cos kx, \\ & \sin\phi[-\cos kx + \sin kx] + \cos\phi). \end{aligned} \tag{A.10}$$

We then compute the components of the tetrahedratic order parameter, $T_{ijk}$, with $T_{ijk} = \sum_{a=1}^{4} n_i^a n_j^a n_k^a$,

$$T_{xxx} = \frac{2}{\sqrt{3}} \sin(2\phi)\cos\phi\sin(2kx) \tag{A.11}$$

$$T_{xxy} = -T_{zzy} = \frac{4}{3\sqrt{3}} \sin(2\phi)\cos(2kx) \tag{A.12}$$

$$T_{xxz} = \frac{4}{3\sqrt{3}} \cos\phi\,(2\sin^2\phi - \cos^2\phi)\sin(2kx) \tag{A.13}$$

$$T_{xyy} = -\frac{4}{3\sqrt{3}} \sin\phi\sin(2kx) \tag{A.14}$$

$$T_{xyz} = -\frac{4}{3\sqrt{3}} \cos(2\phi)\cos(2kx) \tag{A.15}$$

$$T_{xzz} = \frac{4}{3\sqrt{3}} \sin\phi\,(\sin^2\phi - 2\cos^2\phi)\sin(2kx) \tag{A.16}$$

$$T_{yyy} = 0 \tag{A.17}$$

$$T_{yyz} = \frac{4}{3\sqrt{3}} \cos\phi\sin(2kx) \tag{A.18}$$

$$T_{zzz} = -\frac{2}{\sqrt{3}} \sin(2\phi)\sin\phi\sin(2kx) \tag{A.19}$$

where all other components follow by permutation of the indices.

For the components of the nematic orientational order parameter $Q_{ij} = \frac{S}{2}(3n_i n_j - \delta_{ij})$ of the splay-bend texture we get from Eq.(2)

$$Q_{zz} = \frac{S}{2}(3\alpha^2 - 1) \tag{A.20}$$

$$Q_{xx} = \frac{S}{2}(3\beta^2\cos^2 qx - 1) \tag{A.21}$$

$$Q_{yy} = \frac{S}{2}(3\beta^2\sin^2 qx - 1) \tag{A.22}$$

$$Q_{xz} = \frac{3}{2} S\alpha\beta \cos qx \tag{A.23}$$

$$Q_{yz} = \frac{3}{2} S\alpha\beta \sin qx \tag{A.24}$$

$$Q_{xy} = \frac{3}{2} S\beta^2 \sin qx \cos qx \tag{A.25}$$

These expressions are used in the main text to calculate the gradient energy of the splay-bend texture.

## Appendix B: The special case of a homogeneous energy density

In this appendix we will consider a structure with a constant energy density, which is, however, not the absolute minimum state.

For $k = \pm q$ and

$$3\cos^2\phi \pm 4\cos\phi + 1 = 0 \tag{B.1}$$

we obtain from Eq.(10) an expression that is constant in space and, thus, a finite contribution to the energy (7). Eq.(B.1) leads to the solutions

$$\cos\phi = \mp\frac{1}{3} \tag{B.2}$$

for $k = \pm q$ and

$$\sin\phi = \pm\frac{2\sqrt{2}}{3} \tag{B.3}$$

since the other solutions ($\cos\phi = \pm 1$, $\sin\phi = 0$) lead to a vanishing linear gradient contribution (10). We note that the two values given in Eq.(B.2) correspond to the dihedral angle (70.53°) and the tetrahedral angle, respectively, for the positive sign in Eq.(B.3), and to 289.47° and 250.53°, respectively.

As a result we obtain for the linear gradient term the negative energy contribution

$$\mathcal{D} T_{ijk} \nabla_k Q_{ij} = -2|\mathcal{D}|Sq \tag{B.4}$$

for $\mathcal{D} > 0$ with $\phi = 70.53°$ ($k = q$) or $\phi = 250.53°$ ($k = -q$) and for $\mathcal{D} < 0$ with $\phi = 289.47°$ ($k = q$) or $\phi = 109.47°$ ($k = -q$).

Minimization of the resulting gradient terms in the energy (Eqs.(8), (9) and (B.4)) with respect to the wave vector, $q$, gives the result

$$q_c = \frac{|\mathcal{D}|S}{\frac{9}{2}\gamma S^2 + \frac{128}{9}\delta} \tag{B.5}$$

which is again a wave vector directly proportional to $|\mathcal{D}|$, but slightly smaller than the minimal wave vector (17). Inserting this value into Eq.(B.4) we find a reduction of the energy (7) by $\frac{\mathcal{D}^2 S^2}{\frac{9}{2}\gamma S^2 + \frac{128}{9}\delta}$, which is only slightly smaller than the true minimal case Eq.(18).

We thus arrive at the conclusion that the largest energy reduction is obtained by a state with spatially varying energy density. Remarkably, ca. 80% of the maximum energy reduction can be obtained by a state of spatially homogeneous energy density, which features $\phi$-values corresponding to the tetrahedral and dihedral angles, respectively.

## References


1. L.G. Fel, *Phys. Rev. E* **52**, 702 (1995).
2. L. Radzihovsky and T.C. Lubensky, *Europhys. Lett.* **54**, 206 (2001).
3. Throughout the present manuscript we focus on the nonchiral tetrahedratic phase, $T_d$ [1]. We note, however, that our analysis is also useful for the blue phase version of its chiral analogue, the $T$ phase [1].
4. H.R. Brand, P.E. Cladis and H. Pleiner, *Macromolecules* **25**, 7223 (1992).
5. P.E. Cladis and H.R. Brand, *Liq. Cryst.* **14**, 1327 (1993).
6. T. Niori, T. Sekine, J. Watanabe, T. Furukawa, H. Takezoe, *J. Mat. Chem.* **6**, 1231 (1996).
7. T. Sekine, T. Niori, J. Watanabe, T. Furukawa, S.W. Choi, H. Takezoe, *J. Mat. Chem.* **7**, 1307 (1997).
8. D.R. Link, G. Natale, R. Shao, J.E. Mclennan, N.A. Clark, E. Körblova, D.M. Walba, *Science* **278**, 1924 (1997).
9. H.R. Brand, P.E. Cladis and H. Pleiner, *Eur. Phys. J. B* **6**, 347 (1998).
10. R. Macdonald, F. Kentischer, P. Warnick, and G. Heppke, *Phys. Rev. Lett.* **81**, 4408 (1998).
11. D. Shen, S. Diele, I. Wirth, and C. Tschierske, *Chem. Commun.* **1998**, 2573 (1998).
12. G. Pelzl, S. Diele and W. Weissflog, *Adv. Mat.* **11**, 707 (1999).
13. P.E. Cladis, H.R. Brand and H. Pleiner, *Liquid Crystals Today* **9 (3/4)**, 1 (1999).
14. H.R. Brand, P.E. Cladis and H. Pleiner *Int. J. Eng. Sci.* **38**, 1099 (2000).
15. P.E. Cladis, H. Pleiner and H.R. Brand, *Ferroelectrics* **243**, 221 (2000).
16. H. Pleiner, H.R. Brand and P.E. Cladis, *Ferroelectrics* **243**, 291 (2000).
17. G. Pelzl, S. Diele, S. Grande, A. Jakli, Ch. Lischka, H. Kresse, H. Schmalfuss, I. Wirth and W. Weissflog, *Liq. Cryst.* **26**, 401 (1999).
18. P.G. de Gennes, *Mol. Cryst. Liq. Cryst.* **12**, 191 (1971).
19. T.C. Lubensky and L. Radzihovsky, *Phys. Rev. E* **66**, 031704 (2002).
20. P.E. Cladis, *Tetrahedratic Order in Biological Systems*, Invited Symposium M5b *Tetrahedratic (Octupolar) Order in Complex Materials*, American Physical Society, Los Angeles, CA, March 22, 2005, *Bull. Am. Phys. Soc.*, available on-line.
21. H.R. Brand, H. Pleiner and P.E. Cladis, *Physica A* **351**, 189 (2005).
22. H.R. Brand, H. Pleiner and P.E. Cladis, *Eur. Phys. J. E* **7**, 163 (2002).
23. P.E. Cladis, W. Weissflog, G. Pelzl and H.R. Brand, to be published.
24. Y. Yusuf, Y. Hidaka, S. Kai, H.R. Brand, P.E. Cladis, W. Weissflog and G. Pelzl, *Ferroelectrics* **276**, 171 (2002).
25. P.E. Cladis, H. Pleiner and H.R. Brand, *Eur. Phys. J. E* **11**, 283 (2003).
26. W. Weissflog, M.W. Schröder, S. Diele and G. Pelzl, *Adv. Mat.* **15**, 630 (2003).
27. G. Pelzl, A. Eremin, S. Diele, H. Kresse and W. Weissflog, *J. Mat. Chem.* **12**, 2591 (2002).
28. T. Niori, J. Yamamoto and H. Yokoyama, *Mol. Cryst. Liq. Cryst.*, **409**, 475 (2004).
29. M. Hird, Y. Raoul, J.W. Goodby, and H.F. Gleeson, *Ferroelectrics*, **309**, 95 (2004).

30. H.R. Brand, P.E. Cladis and H. Pleiner, *Ferroelectrics*, **315**, 165 (2005).
31. H. Pleiner and H.R. Brand, *Europhys. Lett.* **9**, 243 (1989).
32. D.A. Coleman et al., *Science* **301**, 1204 (2003).
33. F. Grandjean, *Bull. Soc. Mineral.* **42**, 42 (1919). *See also*: P.E. Cladis and A.E. White, *J. Appl. Phys.* **47**, 1256 (1976).
34. G. Toulouse, *J. Physique Lett.* **38**, L-67 (1977), G.E. Volovik and V.P. Mineev, Sov. Phys. *JETP* **45**, 1186 (1977). *See also*: N. D. Mermin, Rev. Mod. Phys. **51**, 591 (1979).
35. L.A. Madsen, T. J. Dingemans, M. Nakata and E.T. Samulski, Phys. Rev. Lett. **92**, 145505 (2004).
36. B. Acharya, A. Primak and S. Kumar, Phys. Rev. Lett. **92**, 145505 (2004).